

# Synaptic Drive onto Inhibitory and Excitatory Principal Neurons of the Mouse Lateral Superior Olive

Hariprakash Haragopal,<sup>1</sup> Mara J. Voytek,<sup>1</sup> and  Bradley D. Winters<sup>1,2</sup>

<sup>1</sup>Department of Biological Sciences and University Hospitals – NEOMED Hearing Research Center, Northeast Ohio Medical University, Rootstown, Ohio, 44272 and <sup>2</sup>Brain Health Research Institute, Kent State University, Kent, Ohio, 44242

## Abstract

Principal neurons (PNs) of the lateral superior olive (LSO) are a critical component of brain circuits that compare information between the two ears to extract sound source-location-related cues. LSO PNs are not a homogenous group but differ in their transmitter type, intrinsic membrane properties, and projection pattern to higher processing centers in the inferior colliculus. Glycinergic inhibitory LSO PNs have higher input resistance than glutamatergic excitatory LSO PNs (~double). This suggests that the inhibitory cell type has a lower minimum input or signal intensity required to produce an output (activation threshold) which may impact how they integrate binaural inputs. However, cell-type-specific differences in the strength of synaptic drive could offset or accentuate such differences in intrinsic excitability and have not been assessed. To evaluate this possibility, we used a knock-in mouse model to examine spontaneous and electrically stimulated (evoked) synaptic events in LSO PN types using voltage-clamp technique. Both excitatory and inhibitory spontaneous postsynaptic currents were larger in inhibitory LSO PNs, but evoked events were not. Additionally, we found that LSO PN types had inputs with similar short-term plasticity and number of independent fibers. An important contrast was that inhibitory LSO PNs received inhibitory inputs with slower decay kinetics which could impact integrative functions. These data suggest that synaptic inputs onto LSO PNs are unlikely to offset excitability differences. Differences in activation threshold along with transmitter type and projection laterality may allow for distinct roles for LSO PN types in inferior colliculus information processing.

**Key words:** auditory; brainstem; lateral superior olive; sound localization

## Significance Statement

Lateral superior olive (LSO) neurons compare information between the two ears to extract location-related cues. LSO neurons differ in the transmitters they release and their projection pattern to higher processing centers, but their relative functions, synapses, and targets are not fully understood. Inhibitory LSO neurons have higher intrinsic excitability, requiring less current to drive them to fire action potentials, but it was not known whether there are cell-type-specific synaptic input differences that offset or accentuate their excitability differences. We found that the synaptic inputs to these neurons have largely similar strength, number, and short-term plasticity. This suggests that membrane excitability differences between LSO neuron types are an important factor for understanding transfer of LSO information to higher processing centers.

## Introduction

Interaural time and level differences (ITDs, ILDs) are useful for horizontal/azimuth sound localization. Circuits in the brainstem of mammals compare synaptic inputs driven by each ear to extract this information. Principal neurons (PNs) of the lateral superior olive (LSO) are distinct from olivocochlear neurons found in the same region in rodents and project via the

Received March 3, 2025; revised April 11, 2025; accepted April 18, 2025.

The authors declare no competing financial interests.

Author contributions: B.D.W. designed research; H.H., M.J.V., and B.D.W. performed research; H.H. and B.D.W. analyzed data; H.H. and B.D.W. wrote the paper.

We thank Dr. Joshua H. Goldwyn for valuable input on data analysis and the manuscript. This work was supported by the United States National Institutes of Health, Institute on Deafness and Other Communication Disorders R56DC020937 and R01DC020937 Winters.

*Continued on next page.*

lateral lemniscus to the inferior colliculus (IC; Sterenborg et al., 2010; Friauf et al., 2019; Williams et al., 2022; Frank et al., 2023; Maraslioglu-Sperber et al., 2024). These neurons compare excitatory inputs driven by the ipsilateral ear and inhibitory inputs driven by the contralateral ear. In this canonical circuit, ipsilateral excitation comes directly from glutamatergic spherical bushy cells in the anteroventral cochlear nucleus (AVCN) while inhibitory inputs arrive via the glycinergic relay neurons in the ipsilateral medial nucleus of the trapezoid body (MNTB) which are driven by globular bushy cells in the contralateral AVCN (for review, see Grothe et al., 2010; Friauf et al., 2019; Joris and van der Heijden, 2019; Yin et al., 2019). Subtractive analysis of these inputs gives LSO PNs intrinsic sensitivity to ITDs and ILDs (Joris and Yin, 1995; Tollin, 2005). Classically the role of LSO PNs was thought to be detection of ongoing ILDs (Tsuchitani and Boudreau, 1966; Boudreau and Tsuchitani, 1968; Tsuchitani, 1977); however, their function in detection of ITDs for the beginning of sounds (onsets), amplitude modulations, and transient broadband sounds is increasingly appreciated (Beiderbeck et al., 2018; Franken et al., 2018, 2021; Joris and Russell, 2018; Ono et al., 2020; Chen and Song, 2024) and there may be cellular diversity to support both roles in the LSO PN population (Haragopal and Winters, 2023).

Not only does the function of LSO PNs depend on the relative weight of their inhibitory and excitatory inputs encoding a location, but the LSO PNs themselves also consist of inhibitory (glycinergic) and excitatory (glutamatergic) transmitter types (Glendenning et al., 1992; Henkel and Brunso-Bechtold, 1995; Fredrich et al., 2009; Ito and Oliver, 2010; Ito et al., 2011; Mellott et al., 2021). In mice, glycinergic cells make up 39% of the population and glutamatergic cells make up 61% (Haragopal et al., 2023).

Inhibitory and excitatory LSO PNs also have different projection patterns to higher processing centers in the IC. In C57BL6/J mice and rats, LSO outputs are fully segregated with inhibition being ipsilateral and excitation contralateral (Ito and Oliver, 2010; Haragopal et al., 2023; but see Williams and Ryugo, 2024); however, low-frequency-hearing cats and Mongolian gerbils have both contralateral and ipsilateral excitatory LSO projections (Glendenning et al., 1992; Henkel and Brunso-Bechtold, 1995; Fredrich et al., 2009; Mellott et al., 2021). Prior studies have examined synaptic inputs to the LSO, but not with respect to the different PN types and largely from a developmental perspective (Sanes and Rubel, 1988; Sanes, 1990; Wu and Kelly, 1992; Sanes, 1993; Gillespie et al., 2005; Kandler et al., 2009; Noh et al., 2010; Case and Gillespie, 2011; Pilati et al., 2016; Gjoni et al., 2018b).

LSO PNs differ in their intrinsic membrane properties; however, their synaptic inputs have not been compared. Questions remain about how the combined synaptic and intrinsic properties of these two types of LSO PNs impact sound localization and higher auditory processing. Inhibitory LSO PNs have substantially higher input resistances (~double on average) and correspondingly lower minimum current injection needed to elicit an action potential (rheobase), suggesting they have a lower minimum input or signal intensity required to produce an output (activation threshold) than excitatory LSO PNs (Haragopal and Winters, 2023). How this relates to LSO circuit function would depend on whether there are cell-type-specific differences in synaptic drive that might offset or accentuate intrinsic excitability differences. To determine whether this is the case, we made whole-cell recordings from identified LSO PN types in voltage-clamp mode and recorded spontaneous and electrically stimulated synaptic responses using synaptic blockers to isolate glycinergic inhibitory and glutamatergic excitatory inputs.

We found several cell-type-specific differences in synaptic drive but also many similarities. Inhibitory LSO PNs exhibited larger amplitude spontaneous excitatory and inhibitory events, but not evoked events. Spontaneous event frequencies and the number of single input fibers were similar between LSO PN types. These data suggest that cell type-specific synaptic drive does not offset intrinsic membrane excitability differences between LSO PN types and that the inhibitory LSO PNs likely have lower activation thresholds within the canonical LSO circuit. We also observed slower decay kinetics in inhibitory LSO PNs which may differentially affect integrative synaptic functions. Together, these data clarify previously observed excitability differences and lay the groundwork for future modeling and in vivo studies.

## Materials and Methods

**Animals.** All animal procedures were approved by the Northeast Ohio Medical University Animal Care and Use Committee in accordance with the guidelines of the

Correspondence should be addressed to Bradley D. Winters at bwinters@neomed.edu.

Copyright © 2025 Haragopal et al. This is an open-access article distributed under the terms of the Creative Commons Attribution 4.0 International license, which permits unrestricted use, distribution and reproduction in any medium provided that the original work is properly attributed.

United States National Institutes of Health. Mice were procured from Jackson Labs. We produced vGlut2 reporter mice by crossing a vGlut2-cre mouse line (B6J.129S6[FVB]-Slc17a6<sup>tm2(cre)Low</sup>/MwarJ; RRID: IMSR\_JAX:028863) with Ai9 tdTomato reporter mice [B6.Cg-Gt(ROSA)26Sort<sup>m9(CAG-tdTomato)Hze</sup>/J; RRID: IMSR\_JAX:007909] to obtain red fluorescent labeling of vGlut2-expressing cells. Animals were then bred at Northeast Ohio Medical University maintaining a 12 h light cycle with *ad libitum* food and water. Animals of both sexes were used (62 male and 44 female). At the time of electrophysiological recordings, mice were aged 26–50 d ( $40 \pm 0.6$  average). There was no difference in age between LSO PN transmitter types (vGlut2+:  $40.34 \pm 0.75$  d,  $n = 55$ ; vGlut2–:  $39.96 \pm 0.82$  d,  $n = 51$ ,  $p = 0.73$ ,  $t$  test).

**Electrophysiology.** Animals were transcardially perfused under isoflurane anesthesia with oxygenated, room temperature cutting solution containing the following (in mM): 135 *N*-methyl-D-glucamine (NMDG, Sigma), 1.25 KCl, 1.25 KH<sub>2</sub>PO<sub>4</sub>, 0.5 CaCl<sub>2</sub>, 2.5 MgCl<sub>2</sub>, pH 7.35 with HCl,  $\sim 310$  mmol/kg then decapitated and the brain quickly removed. The brainstem was isolated, embedded in 1% agarose, and sliced coronally 200–230  $\mu$ m thick using a vibrating microtome (7000 smz2, Campden) at room temperature. Slices were transferred to a recovery solution containing the following (in mM): 110 NaCl, 2.5 KCl, 1.5 CaCl<sub>2</sub>, 1.5 MgCl<sub>2</sub>, 25 NaHCO<sub>3</sub>, 1.25 NaH<sub>2</sub>PO<sub>4</sub>, 12 dextrose, 5 *N*-acetyl-L-cysteine, 5 Na-ascorbate, 3 Na-pyruvate, 2 thiourea, pH 7.35 with NaOH, continuously bubbled with 5% carbogen,  $\sim 295$  mmol/kg at 35°C for 30 min and then maintained at room temperature until being transferred to the recording stage. Recordings were made in oxygenated artificial cerebrospinal fluid (ACSF) containing the following (in mM): 120 NaCl, 2.5 KCl, 1.5 CaCl<sub>2</sub>, 1.5 MgCl<sub>2</sub>, 25 NaHCO<sub>3</sub>, 1.25 NaH<sub>2</sub>PO<sub>4</sub>, 12 dextrose, pH 7.35 with NaOH,  $\sim 295$  mmol/kg at  $35 \pm 0.5^\circ\text{C}$  maintained using an in-line heating system.

Neurons were targeted using differential interference contrast microscopy combined with widefield fluorescence (Axioskop 2 FS Plus, 40 $\times$  NA 0.8 objective, Zeiss). LSO PNs were distinguished from olivocochlear cells based on size and shape. LSO neurons that are larger, fusiform-shaped cells are highly likely (>95%) to be PNs with prominent  $I_h$  sag currents and lacking the A-current delay-to-firing response associated with olivocochlear cells (Adam et al., 1999; Sterenborg et al., 2010; Williams et al., 2022; Maraslioglu-Sperber et al., 2024).

Whole-cell patch-clamp recordings were made using Dual IPA (Sutter Instrument) or EPC-10 USB (HEKA) amplifiers with integrated digitizers in voltage-clamp mode using thick-walled borosilicate patch pipettes (2–4 M $\Omega$ , Sutter Instrument) filled with Cs-based internal containing the following (in mM): 40 CsMeSO<sub>3</sub>, 70 CsCl, 5 EGTA, 10 HEPES, 10 Na<sub>2</sub> phosphocreatine,  $\sim 8$  sucrose, 2 Mg-ATP, 0.3 Na-GTP, 1.8 CaCl<sub>2</sub>, 1.5 QX-314 (HBr), 0.02 ZD 7288, 5 4-AP, 10 TEA-Cl, 0.1% (2.68 mM) biocytin, pH 7.30 with CsOH,  $\sim 295$  mmol/kg,  $E_{\text{Cl}} = -12$  mV at 35°C. Data were low-pass filtered at 5 or 2.9 kHz, digitized at 20–50 kHz, and acquired to computer using PatchMaster Next (HEKA) or SutterPatch (Sutter Instrument). A calculated liquid junction potential of  $-6$  mV was corrected. Resting membrane potential was recorded immediately after break-in. Cells were held at  $-70$  mV during synaptic data collection.

$\alpha$ -amino-3-hydroxy-5-methyl-4-isoxazolepropionic acid receptor (AMPA)-mediated glutamatergic inputs were isolated by bath-applied pharmacological blockade of glycine receptors (1  $\mu$ M strychnine, Sigma), GABA<sub>A</sub> receptors (2  $\mu$ M gabazine, Sigma), GABA<sub>B</sub> receptors (1  $\mu$ M CGP55845, Sigma), and NMDA receptors (25  $\mu$ M D-AP5, Alomone Labs). Glycine receptor (GlyR)-mediated inhibition was isolated by bath-applied pharmacological blockade of GABA<sub>A</sub> receptors (2  $\mu$ M gabazine, Sigma), GABA<sub>B</sub> receptors (1  $\mu$ M CGP55845, Sigma), NMDA receptors (25  $\mu$ M D-AP5, Alomone Labs), and AMPA/kainite receptors (10  $\mu$ M NBQX, Alomone Labs).

**Spontaneous synaptic events.** Spontaneous events were analyzed from 9 to 31 s long raw traces acquired at 50 kHz (excitation, mean  $117 \pm 17$  events/cell; inhibition,  $415 \pm 55$  events/cell). Spontaneous events were detected using a custom MATLAB GUI platform. Semiautomated detection used an estimate of the noise floor obtained by subtracting a low-pass filtered version of the raw trace (fourth-order Butterworth at 1.25 kHz cutoff) from the raw trace and a manual threshold for deviation. Exclusion of spurious events, inclusion of missed events, and rewindowing of detected events as well as separation of compound events was done manually. Peaks of compound events were counted in frequency analysis, but only single events were used for amplitudes and kinetics. Amplitude was calculated from a local baseline immediately before the event. Amplitude averages provide information on the typical strength of postsynaptic responses. Cumulative frequency distributions provide more details. These distributions can reveal the presence of multiple channel subtypes if bimodal or multimodal and help characterize the variability due to quantal parameters. Kinetic parameters analyzed were 20–80% rise times, halfwidths (event width at half amplitude), and decay time constant ( $\tau$ ). Series resistance ( $R_s$ ) was monitored with a  $-6$  mV hyperpolarizing test pulse at the start of each sweep and cells were excluded if  $R_s$  changed by >30%.

**Evoked synaptic responses.** A glass stimulating electrode ( $\sim 20$   $\mu$ m inner diameter, WPI) was placed either lateral to LSO near the seventh nerve to stimulate fibers of the ventral acoustic stria for excitatory synaptic inputs or medial to the LSO to stimulate fibers from the MNTB for inhibitory synaptic inputs. Stimulation pulses were delivered with a stimulus isolator (WPI A-395 or Digitimer DS4) controlled by the recording amplifier.  $R_s$  was monitored with a  $-6$  mV hyperpolarizing test pulse at the start of each sweep and cells were excluded if  $R_s$  changed by >30%. Minimal stimulation (>12% failures) was 40–100  $\mu$ s duration and 40 sweeps recorded at a sampling rate of 20–50 kHz. For paired pulses, 40–100 repetitions were recorded with a 2 s intersweep interval. Responses were filtered with a fourth-order low-pass Butterworth filter with a

cutoff of 1.25 kHz (single pulse) or 1.5 kHz (paired pulse). Response kinetics were evaluated using 20–80% rise times, half-width, and decay time constant. Paired-pulse ratios were determined as the ratio of the second to the first pulse response amplitude. For PPRs, cells were only included if they had at least seven trials with responses to both stimuli.

For wide stimulation range experiments, stimulation durations were 100  $\mu$ s and incrementally increased at a fixed step size for current amplitudes up to 10 mA or until LSO PN responses saturated. If synaptic responses did not saturate or the baseline was more negative than  $-200$  pA, cells were discarded. Here, a more stringent criterion of  $R_s < 20\%$  change was applied where  $R_s$  was measured from a hyperpolarizing voltage step of  $-10$  mV applied at the beginning of a sweep. Raw traces were used for input count estimation. A further inclusion criterion applied was the absence of spontaneous or compound events in the response window. The average of a 10 ms window prior to the first pulse was used as baseline for estimating response amplitudes.

For a given neuron, the number of synaptic inputs were estimated from postsynaptic current (PSC) amplitude distribution fits using a Gaussian mixture model (GMM; Lee et al., 2023). The PSC amplitude distributions were modeled as having been generated by a latent mixture of normally distributed components, with each component contributing a specific mean amplitude and variance to the overall distribution. A sum of the Gaussians of each component weighted by its prior probability provided the fit. To arrive at the fit, the PSC amplitude distributions were first fitted with 1–20 components using the `fitgmdist()` function in MATLAB based on an expectation-maximization (EM) algorithm running on PSC amplitudes. For each component of a  $k$ -component Gaussian mixture, an initial PSC amplitude was chosen at random from the data as its mean, where the default initialization method or “plus” in `fitgmdist()` ensured that the chosen values are as far apart as possible for improved clustering, and the variance of PSC amplitudes was treated as a diagonal element of a  $k$ -by- $k$  diagonal covariance matrix and was identical for all the  $k$  components. In the expectation step, posterior probability for membership of each PSC amplitude to each component was computed using these initial values, assuming a uniform prior probability,  $1/k$  for  $k$  components. In the maximization step, the posterior probabilities were used as weights in computing component means, covariance matrix, and mixing proportions based on the maximum likelihood approach. In the ensuing expectation step, the mixing proportions served as prior probabilities and were used along with the means and covariance matrix for updating posterior probabilities. A maximum EM iteration of 1,500 ensured that the loglikelihoods of the  $k$ -component GMM fits were stable to within a tolerance of  $1 \times 10^{-7}$ . The estimation of the loglikelihood function for the GMM fit required the determinant of the covariance matrix that had only diagonal entries to go into the denominator. The determinant must not be zero or assume near-zero values to avoid infinite or large loglikelihoods to ensure stable fits. Thus, at each EM iteration, a non-negative regularization value of 0.01 was added to the diagonal entries of the covariance matrix and this matrix was shared by all inputs. To identify the optimal input number, Bayesian information criterion (BIC) was computed from the loglikelihood of the GMM fit. The GMM fit was considered optimal among all  $k$ -component GMM fits, if for any  $k$ , ranging from 1 through 20 components, the BIC was 20 over the minimum value (Lee et al., 2023) and had a component count estimate larger than that allowed by minimum BIC. This provided a tradeoff between overfitting and underfitting of the distribution by the model. Then, to further penalize overfitting, the number of inputs were conservatively determined as the number of modes or peaks in the fits, as these were always smaller than the number of components. Modes were identified from fits plotted using MATLAB function `pdf()` at fixed bin intervals of 93 pA for synaptic inhibition and at fixed intervals of 36 pA for synaptic excitation. All modes were counted regardless of their prominence as this parameter is affected by the sum of the underlying Gaussian components. The chosen bin widths above were derived from the 25th percentiles for response amplitudes for minimal stimulation, estimated more conservatively by excluding those with large amplitudes  $>1$  nA to capture contributions from single fibers. Single fiber inputs to LSO are likely to have multiple synaptic contacts (Cant, 1984; Gjoni et al., 2018a). Minimal and maximal stimulation amplitudes used for ratiometric input counts were the smallest and largest amplitudes at which peaks were detected by our algorithm, respectively.

**Statistics.** Statistical comparisons were made using Prism (GraphPad) or MATLAB. The data are shown as mean  $\pm$  SEM along with the data points. Significance was assessed using an alpha level of 0.05. The data points for synaptic measurements themselves were the average of across sweep measurements for each LSO PN and statistical inferences were mainly based on these average measurements. Comparisons between transmitter types were made on these data points using two-tailed, unpaired  $t$  test. Spearman’s  $r$  was used to test correlation of parameters. Cumulative spontaneous event amplitude distributions were tested using the Kolmogorov–Smirnov test.

Paired-pulse stimulation was carried out at minimal stimulation intensities to better assess short-term synaptic plasticity by only activating the same synapses. At minimal intensity, events are small and the number of trials with both first and second events could be low (minimum of 7 for inclusion). A bootstrap test was performed at an alpha level of 0.05 on the paired-pulse data from individual neurons to test whether the average paired-pulse ratios (PPRs) were borne out of an interaction of the first pulse response with those of the second pulse and not simply due to variability in responses to the first pulse. For this, a test of interaction was carried out based on bootstrapped mean PPRs where the null distribution for mean PPRs were generated with first pulse alone. A single instance of bootstrap sampling had the same number of trials that went into calculation of average PPR for the neuron. This yielded 1,000 such instances from which mean PPRs were computed, and a null distribution was constructed from the 1,000 mean PPRs calculated. This gave at least seven traces from which bootstrap distributions could be created and at least 49 unique pairs with 1,000 iterations gave sufficient

sampling for neurons with larger number of traces. Thus, the  $p$  value was the probability of seeing in the null distribution at least the mean PPR value (if  $> 1$ ) or at most the mean PPR value (if  $< 1$ ) computed from data.

## Results

### Excitatory inputs

We used knock-in vGlut2 reporter mice to identify fluorescent excitatory LSO PNs and nonexpressing inhibitory LSO PNs by subtractive logic (Haragopal and Winters, 2023) for whole-cell voltage-clamp recordings. Since the cochlear nuclei are removed in our preparation, there is little to no action potential-driven activity in inputs to LSO PNs; therefore, spontaneous synaptic events are a good general measure of the relative number (frequency) and strength (amplitude) of synaptic inputs from all sources. Pharmacologically isolated AMPAR-mediated glutamatergic spontaneous excitatory postsynaptic currents (sEPSCs; Fig. 1*A,B*) exhibited larger average amplitudes in inhibitory LSO PNs [excitatory LSO PNs (E):  $20.90 \pm 1.60$  pA, inhibitory LSO PNs (I):  $26.66 \pm 2.00$  pA,  $t$  test,  $p = 0.04$ , Fig. 1*D*] and the cumulative probability distribution was also substantially shifted toward larger events in inhibitory LSO PNs (KS test,  $D = 0.1077$ ,  $p < 0.001$ , Fig. 1*C*). The frequency of sEPSCs was similar between LSO PN types (E:  $10.9 \pm 3.2$  Hz, I:  $10.3 \pm 1.9$  Hz,  $t$  test,  $p = 0.90$ , Fig. 1*E*) as were their kinetics (rise: E:  $0.160 \pm 0.004$  ms, I:  $0.150 \pm 0.008$  ms,  $t$  test,  $p = 0.35$ , Fig. 1*F*; halfwidth: E:  $0.730 \pm 0.040$  ms, I:  $0.690 \pm 0.046$  ms,  $t$  test,  $p = 0.52$ , Fig. 1*G*; decay: E:  $0.76 \pm 0.05$  ms, I:  $0.75 \pm 0.08$  ms,  $t$  test,  $p = 0.93$ , Fig. 1*H*).

Minimal evoked EPSCs stimulated near the seventh nerve (eEPSCs, 12–90% failure rate, Fig. 2*A*) had similar average amplitude between LSO PN types (E:  $120.2 \pm 66.1$  pA, I:  $233.3 \pm 118.9$  pA,  $t$  test,  $p = 0.46$ , Fig. 2*B*, left and smaller events at expanded scale, 2*B*, right) and included some cells with very large single fiber amplitudes in excess of 1 nA despite meeting our failure rate criteria. If we were to exclude these 3 data points, the averages would be much smaller but still not significantly different (E:  $54.23 \pm 5.5$  pA, I:  $63.90 \pm 9.6$ ,  $t$  test,  $p = 0.43$ , data not shown). We did not observe differences in minimal eEPSC kinetics between LSO PN types (rise: E:  $0.36 \pm 0.03$  ms, I:  $0.32 \pm 0.02$  ms,  $t$  test,  $p = 0.26$ , Fig. 2*C*; halfwidth: E:  $1.36 \pm 0.15$  ms, I:  $1.29 \pm 0.17$  ms,  $t$  test,  $p = 0.77$ , Fig. 2*D*; decay: E:  $1.27 \pm 0.17$  ms, I:  $1.22 \pm 0.20$  ms,  $t$  test,  $p = 0.85$ , Fig. 2*E*).

We examined the paired-pulse ratio of minimal eEPSCs at three interpulse intervals (IPIs, 5, 10, and 20 ms). At 5 ms IPI, the average ratios were similar between LSO PN types and slightly above 1 (E:  $1.30 \pm 0.07$ , I:  $1.40 \pm 0.20$ ,  $t$  test,  $p = 0.56$ , one-sample  $t$  test for all PPRs shown vs PPR of 1,  $p = 0.0082$ , Fig. 2*F*). At larger IPIs there appeared to be little interaction between events and no differences between LSO PN types (10 ms IPI: E:  $1.07 \pm 0.09$ , I:  $1.18 \pm 0.13$ ,  $t$  test,  $p = 0.56$ , one-sample  $t$  test for all PPRs shown vs PPR of 1,  $p = 0.13$ , Fig. 2*G*; 20 ms IPI: E:  $1.02 \pm 0.07$ , I:  $1.02 \pm 0.06$ ,  $t$  test,  $p = 0.94$ , one-sample  $t$  test for all PPRs shown vs PPR of 1,  $p = 0.62$ , Fig. 2*H*). We used minimal stimulation for our PPR analysis to ensure interaction at the same synapses. Thus, there were a lot of trials with failures. In some cases, the number of trials in which responses to both first and second stimulation were present was relatively small (at least seven trials to be accepted). Additionally, minimal stimulation events are usually quite small amplitude raising the question of how random amplitude variability might influence PPR on a trial-by-trial basis. This might draw the computed mean PPR value away from the true mean PPR value regardless of event interaction. To address this possibility, we ran an analysis in which

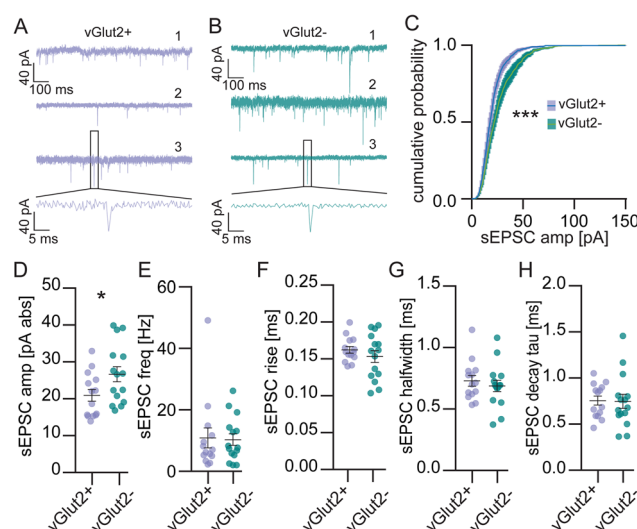


**Figure 1.** Spontaneous excitatory postsynaptic currents (sEPSCs) are larger in inhibitory LSO PNs. **A**, Example traces from 3 vGlut2 positive (excitatory) LSO PNs. **B**, Example traces from 3 vGlut2 negative (inhibitory) LSO PNs. **C**, Cumulative probability of sEPSC amplitudes. **D**, Amplitude of sEPSCs. **E**, Frequency of sEPSCs. **F**, sEPSC 20 to 80% rise time. **G**, sEPSC halfwidths. **H**, sEPSC decay tau (time constant). Cells (animals) E:  $n = 14(8)$ , I:  $n = 15(12)$ . Mean  $\pm$  SEM. \* $p < 0.05$ , \*\*\* $p < 0.001$ .

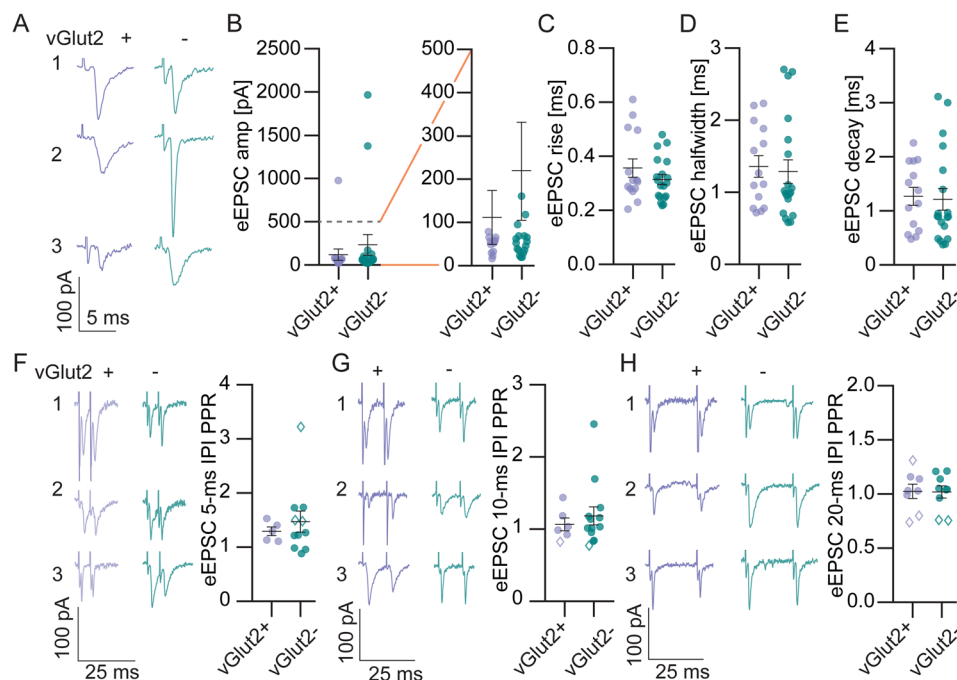


**Figure 2.** Evoked EPSCs (eEPSCs) exhibit similar amplitude, kinetics, and short-term plasticity in LSO PN types. **A**, Example eEPSC traces at minimal stimulation from 3 vGlut2+ (left, excitatory) and 3 vGlut2- (right, inhibitory) LSO PNs. **B**, Minimal eEPSC amplitude (all left and at expanded scale right). **C**, Minimal eEPSC 20–80% rise time. **D**, Minimal eEPSC halfwidth. **E**, Minimal eEPSC decay tau. **B–E**, Cell (animals) E:  $n = 14(10)$ , I:  $n = 19(14)$ . **F**, Example eEPSC traces for a pair of stimulations at minimal stimulation intensity with 5 ms interpulse interval (IPI) from 3 vGlut2+ (left traces) and 3 vGlut2- (right traces) LSO PNs. Scale is the same for all traces. Paired-pulse ratio (right). Open diamonds in graph are cells with  $p < 0.05$  in bootstrap test for individual LSO PN's mean paired-pulse ratios. E:  $n = 5(5)$ , I:  $n = 11(10)$ . **G**, Same as **F**, for 10 ms IPI. E:  $n = 6(5)$ , I:  $n = 13(11)$ . **H**, 20 ms IPI. E:  $n = 8(7)$ , I:  $n = 9(9)$ . Mean  $\pm$  SEM.

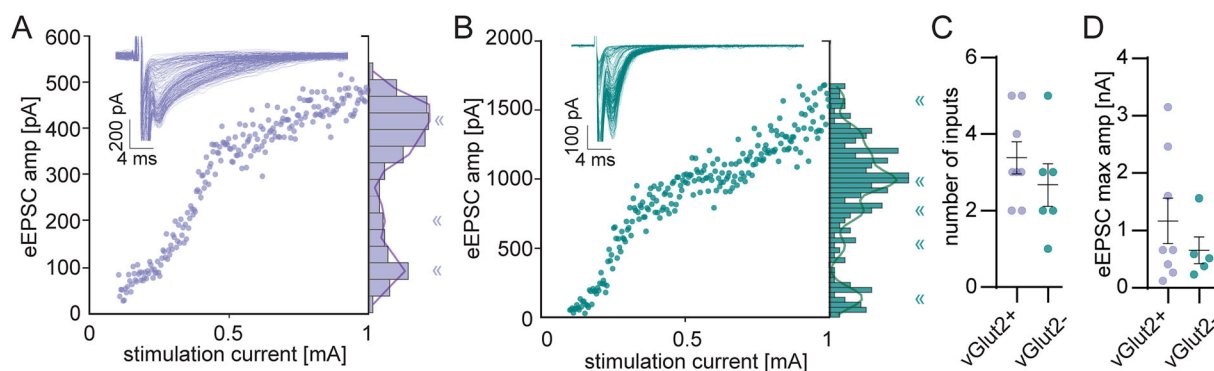


**Figure 3.** LSO PN types receive similar numbers of excitatory inputs. **A**, Example eEPSC amplitudes plotted against stimulation intensities for an excitatory LSO PN. Overlaid response traces shown in inset. Responses saturated at 1 mA. The number of inputs for the neuron was estimated as the number of peaks in a GMM fit to the histograms binned at 36 pA (solid line overlaying histogram), « symbols indicate the local maxima of the fit. **B**, Same as in **A**, but for an inhibitory LSO PN. **C**, The estimated number of inputs. E:  $n = 8(8)$ , I:  $n = 6(6)$ . **D**, Maximal amplitudes, measured as the largest amplitude at which the GMM fit had a peak. One cell that had a single estimated input but  $< 100$  pA amplitude was discarded from maximal stimulation analyses. E:  $n = 7(7)$ , I:  $n = 6(6)$ . Mean  $\pm$  SEM.

for each neuron the mean PPR from first and second events was compared with those from a bootstrapped set of all first events. Only a few LSO PNs exhibited significant interaction of first pulse responses on those of the second pulses (bootstrap test,  $p < 0.05$ , open diamonds, Fig. 2F–H), suggesting that concrete differences in mean PPR were unlikely at the intervals examined.

In a subset of experiments, we examined eEPSCs over a wide range of electrical stimulation levels from minimal to maximum plateau (Fig. 3A,B, insets). We analyzed the number of peaks using a GMM to assess the approximate number of input fibers (Fig. 3A,B) and found that inhibitory and excitatory LSO PNs had similar numbers (E:  $3.4 \pm 0.4$ ; I:  $2.7 \pm 0.6$ ,  $p =$

0.32, Fig. 3C) and similar maximum amplitudes (E:  $1,170.0 \pm 395.6$  pA; I:  $658.8 \pm 235.1$  pA, *t* test,  $p = 0.36$ , Fig. 3D). We analyzed the ratio of maximal to minimal stimulation amplitudes for each neuron and found no difference between LSO PN types (E:  $8.4 \pm 2.2$ ; I:  $4.2 \pm 1.7$ , *t* test,  $p = 0.17$ , data not shown); however, ratiometric estimates were higher than step-counting estimates (paired *t* test,  $p = 0.02$ ). The two methods were well correlated with each other [Spearman ( $r = 0.88$ ,  $p < 0.0001$ ).

### Inhibitory inputs

Pharmacologically isolated GlyR-mediated spontaneous inhibitory postsynaptic currents (sIPSCs; Fig. 4A,B) had similar average amplitudes (E:  $96.8 \pm 11.4$  pA, I:  $106.5 \pm 10.3$  pA, *t* test,  $p = 0.55$ , Fig. 4D); however, the cumulative probability distribution was shifted toward more large events in inhibitory LSO PNs (KS test,  $D = 0.21$ ,  $p < 0.0001$ , Fig. 4C), suggesting there is a population of stronger synapses that are not numerous enough to skew the average. The frequency of sIPSCs were similar between LSO PN types (E:  $44.8 \pm 8.9$  Hz, I:  $40.3 \pm 6.9$  Hz, *t* test,  $p = 0.71$ , Fig. 4E). Rise times for sIPSCs were similar between LSO PN types (E:  $0.19 \pm 0.01$  ms, I:  $0.18 \pm 0.01$  ms, *t* test,  $p = 0.74$ , Fig. 4F); however, inhibitory LSO PNs had slower sIPSC decay kinetics (halfwidth: E:  $0.94 \pm 0.05$  ms, I:  $1.20 \pm 0.07$  ms, *t* test,  $p = 0.0053$ , Fig. 4G; decay: E:  $0.93 \pm 0.05$  ms, I:  $1.28 \pm 0.09$  ms, *t* test,  $p = 0.0008$ , Fig. 4H).

Minimal evoked IPSCs (eIPSCs, 20–95% failure rate, Fig. 5A) stimulated between the MNTB and the LSO had similar average amplitude in LSO PN types (E:  $389.30 \pm 94.94$  pA, I:  $1,003.00 \pm 448.80$  pA, *t* test,  $p = 0.11$ , Fig. 5B, left and smaller events at expanded scale, 5B, right) and included two cells in the inhibitory LSO PN group with very large single fiber amplitudes in excess of 3 nA. If we were to exclude these 2 data points, the averages would be smaller, but still not significantly different (E:  $389.30 \pm 94.94$  pA, I:  $384.80 \pm 99.26$  pA, *t* test,  $p = 0.98$ , data not shown). Similar to what we saw with sIPSCs, minimal eIPSCs had similar rise times in LSO PN types (E:  $0.30 \pm 0.02$  ms, I:  $0.35 \pm 0.01$  ms, *t* test,  $p = 0.14$ , Fig. 5C), but slower decay kinetics in inhibitory LSO PNs (halfwidth: E:  $1.54 \pm 0.11$  ms, I:  $2.20 \pm 0.17$  ms, *t* test,  $p = 0.002$ , Fig. 5D; decay: E:  $1.50 \pm 0.11$  ms, I:  $2.32 \pm 0.21$  ms, *t* test,  $p = 0.0007$ , Fig. 5E).

We examined the paired-pulse ratio of minimal eIPSCs at three interpulse intervals as well. At all IPIs the average PPRs were similar between LSO PN types and not different from 1 (5 ms IPI: E:  $0.91 \pm 0.10$ , I:  $1.20 \pm 0.20$ , *t* test,  $p = 0.19$ , one-sample *t* test for all PPRs shown vs PPR of 1,  $p = 0.92$ , Fig. 5F; 10 ms IPI: E:  $0.98 \pm 0.10$ , I:  $1.22 \pm 0.12$ , *t* test,  $p = 0.17$ , one-sample *t* test for all PPRs shown vs PPR of 1,  $p = 0.48$ , Fig. 5G; 20 ms IPI: E:  $0.96 \pm 0.15$ , I:  $0.93 \pm 0.05$ , *t* test,  $p = 0.87$ , one-sample *t* test for all PPRs shown vs PPR of 1,  $p = 0.60$ , Fig. 5H). There were also few LSO PNs in which there was a significant influence of first pulse responses on those of the second pulses across IPIs (bootstrap test,  $p < 0.05$ , open diamonds, Fig. 5F–H).

Similar to our observations for eEPSCs, wide stimulus range experiments with eIPSCs suggested that inhibitory and excitatory LSO PNs had similar numbers of inputs (E:  $3.1 \pm 0.7$ ; I:  $2.8 \pm 0.7$ , *t* test,  $p = 0.74$ , Fig. 6A–C) and similar maximal amplitudes (E:  $1,322 \pm 343$  pA; I:  $1,516.0 \pm 489.1$  pA, *t* test,  $p = 0.77$ , Fig. 6D). Ratios of maximal to minimal amplitudes on a per cell basis were similar between LSO PN types as well (E:  $5.6 \pm 1.9$ ; I:  $3.9 \pm 1.3$ , *t* test,  $p = 0.46$ , data not shown). Ratiometric estimates were similar to step-counting estimates (paired *t* test,  $p = 0.1$ ) and the two methods were well correlated with each other [Spearman ( $r = 0.79$ ,  $p = 0.0003$ ).

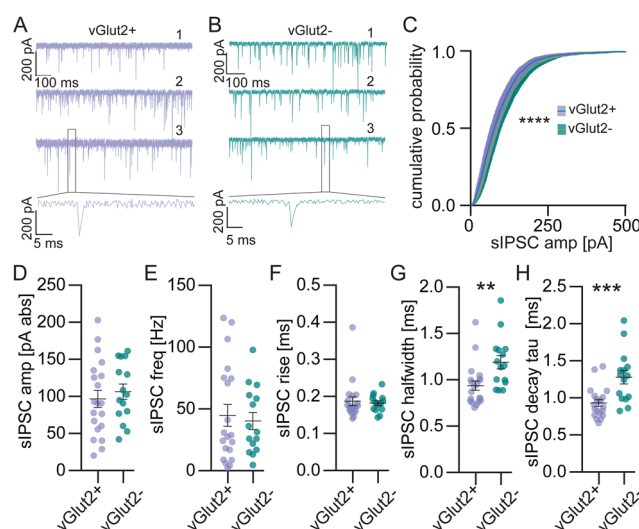


**Figure 4.** Spontaneous inhibitory postsynaptic currents (sIPSCs) have larger amplitudes and slower decay kinetics in inhibitory LSO PNs. **A**, Example traces from 3 vGlut2 positive (excitatory) LSO PNs. High  $\text{Cl}^-$  internal used. **B**, Example traces from 3 vGlut2 negative (inhibitory) LSO PNs. **C**, Cumulative probability of sIPSC amplitudes. **D**, Amplitude of sIPSCs. **E**, Frequency of sIPSCs. **F**, sIPSC 20 to 80% rise time. **G**, sIPSC halfwidths. **H**, sIPSC decay tau (time constant). Cells (animals) E:  $n = 20(15)$ , I:  $n = 15(11)$ . Mean  $\pm$  SEM. \*\* $p < 0.01$ , \*\*\* $p < 0.001$ , \*\*\*\* $p < 0.0001$ .

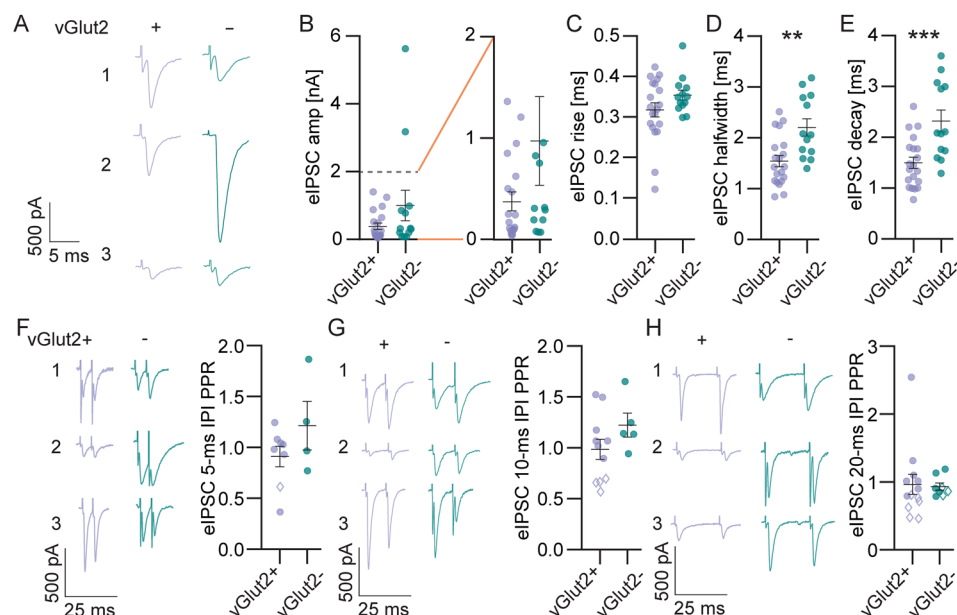


**Figure 5.** Evoked IPSCs (eIPSCs) exhibit slower decay kinetics in inhibitory LSO PN types but similar amplitudes and short-term plasticity between LSO PN types. **A**, Example eIPSC traces at minimal stimulation from 3 vGlut2+ (left, excitatory) and 3 vGlut2- (right, inhibitory) LSO PNs. **B**, Minimal eIPSC amplitude (all left and at expanded scale right). **C**, Minimal eIPSC 20–80% rise time. **D**, Minimal eIPSC halfwidth. **E**, Minimal eIPSC decay tau. **B–E**, Cell (animals) E:  $n = 20(15)$ , I:  $n = 13(10)$ . **F**, Example eIPSC traces for a pair of stimulations at minimal stimulation intensity with 5-ms interpulse interval (IPI) from 3 vGlut2+ (left traces) and 3 vGlut2- (right traces) LSO PNs. Scale is the same for all traces. Paired-pulse ratio (right). Open diamonds in graph are cells with  $p < 0.05$  in bootstrap test for individual LSO PN's mean paired-pulse ratios. E:  $n = 8(8)$ , I:  $n = 4(4)$ . **G**, Same as **F**, for 10 ms IPI. E:  $n = 11(8)$ , I:  $n = 5(5)$ . **H**, 20 ms IPI. E:  $n = 13(10)$ , I:  $n = 8(8)$ . Mean  $\pm$  SEM.  $**p < 0.01$ ,  $***p < 0.001$ .

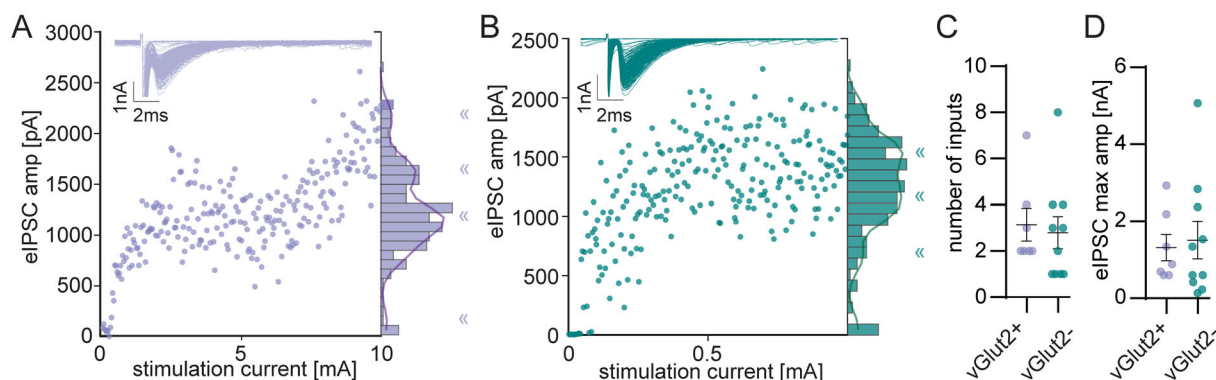


**Figure 6.** LSO PN types receive similar numbers of inhibitory inputs. **A**, Example eIPSC amplitudes plotted against stimulation intensities for an excitatory LSO PN. Overlaid response traces shown in inset. Responses saturated at 10 mA. The number of inputs for the neuron was estimated as the number of peaks in a GMM fit to the histograms binned at 93 pA (solid line overlaying histogram), « symbols indicate the local maxima of the fit. **B**, Same as in **A**, but for an inhibitory LSO PN. Responses saturated at 1 mA. **C**, The estimated number of inputs. **D**, Maximal amplitudes, measured as the largest amplitude at which GMM fit had a peak. E:  $n = 7(6)$ , I:  $n = 10(7)$ . Mean  $\pm$  SEM.

We estimated the whole-cell capacitance of all recorded cells in voltage-clamp mode. We found that inhibitory LSO PNs had smaller capacitance than excitatory LSO PNs (E:  $17.1 \pm 0.6$  pF,  $n = 54$ ; I:  $14.4 \pm 0.5$  pF,  $n = 51$ ;  $t$  test,  $p = 0.0014$ , data not shown).

## Discussion

Our primary objective was to determine if the strength of synaptic drive was similar between LSO PN transmitter types. We did not find any differences between LSO PN types in sEPSC or sIPSC frequency (Figs. 1E, 4E), suggesting they house similar numbers of synapses globally. We did observe that sEPSC amplitudes, both average and cumulative, were larger in inhibitory LSO PNs (Fig. 1C,D). However, we also found that the cumulative distribution of sIPSC amplitudes (Fig. 4C), but not the average (Fig. 4D), were shifted toward larger amplitudes in inhibitory LSO PNs. These data suggest the possibility

that inhibitory LSO PN's stronger excitation and stronger inhibition balance each other out, resulting in no net difference from excitatory LSO PNs. We did not observe differences in minimal eEPSC or eIPSC amplitudes (Figs. 2B, 5B) between LSO PN types. Since these would presumably be the canonical LSO circuit inputs, these data provide further support for the conclusion that the strength of synaptic drive is similar between LSO PN types. Thus, we provide strong evidence that that cell type-specific synaptic drive does not offset the higher intrinsic excitability of inhibitory LSO PNs.

Because of our electrical stimulation locations and synaptic blockers used, noncanonical LSO input sources such as ipsilateral inhibition (Weingarten et al., 2023) and contralateral excitation from nuclei of the trapezoid body (Glendenning et al., 1991) or auditory cortex (Feliciano et al., 1995; Coomes Peterson and Schofield, 2007) would not have been sampled in our evoked synaptic responses. These sources may constitute differences observed between LSO PN types in spontaneous synaptic event amplitudes. Since the function of these inputs is not understood, we cannot speculate as to what such differences might result in.

Some LSO PNs received large minimal/single fiber responses ( $>1$  nA) despite meeting our failure rate criteria (Figs. 2B, 5B). We also observed some cells with large steps in our wide stimulus range experiments, presumably where powerful fibers were recruited above minimal stimulation intensity. The sources of these events are not known, but in the case of excitation may represent a population of cells that receive powerful inputs with multiple boutons, each of which covering multiple synapses, as has been observed in the gerbil medial superior olive (Couchman et al., 2010). Excitatory boutons with multiple synaptic components have also been described for the cat LSO at the EM level (Cant, 1984). In the case of inhibition, powerful inputs with large numbers of active zones have been described for the mouse LSO (Gjoni et al., 2018a). In either case, it is not known if the larger and smaller inputs are from different neuron populations. What we can say is that single fiber amplitudes in the LSO can have a wide range, but we did not observe differences between LSO PN types either including or excluding very large events.

While many studies have described the amplitude of synaptic inputs in LSO, methodological differences complicate direct comparison with our current study. These differences result in substantial variability and stem from the choice of recording mode (voltage-clamp vs current-clamp), developmental age, stimulation intensity, stimulation location, recording temperature, species/strain, ionic composition of external and internal solutions, synaptic blockers for isolation, and the holding potential used. Excellent recent reviews are available on the subject (Friauf et al., 2019; Yin et al., 2019) so we do not attempt to untangle this literature. One study using similar methods (Garcia-Pino et al., 2017) found that P33–35 mice exhibited glutamatergic minimal stimulation amplitudes ( $\sim 50$ – $200$  pA) that are comparable with the range of most of our eEPSCs. Likewise, another recent study (Müller et al., 2022) found minimal eIPSCs amplitudes ( $\sim 150$ – $1,200$  pA) that were similar to our observations, suggesting at least broad agreement with previous reports.

The number of independent inputs to LSO PNs is an important variable for understanding how these cells integrate synaptic drive to extract sound location-related information. Our analysis of wide stimulus range evoked amplitudes suggests that inhibitory and excitatory LSO PN types receive similar numbers of input fibers (Figs. 3C, 6C). This type of electrical stimulation assay is somewhat flawed since it is impossible to say that all fibers were stimulated/differentiated since some number may have been damaged or simply not routed through the stimulation location. Thus, the number of inputs found should be considered a lower bound used to compare between LSO PN types. We also estimated the number of inputs ratiometrically using the maximal amplitude divided by the minimal amplitude for individual neurons. These estimates were also not different between LSO PN types; however, they were larger than our step-counting estimates. This may reflect the occurrence of “multiple fiber steps” despite our small stimulation amplitude step size, thus ratiometric estimates are likely closer to the true number of inputs.

Input fiber count estimates may be affected by multiple methodological parameters such as stimulation or calculation method and there is substantial variability in prior reports. One study found the number for inhibitory inputs to LSO PNs to be  $\sim 4$  at ages P31–49 using a *K*-means clustering method for analyzing staircase responses (Müller et al., 2019). Another prior report using ratiometric analysis of eEPSCs estimated the number of excitatory inputs to be  $\sim 9$  (Garcia-Pino et al., 2017). Ratiometric estimates using optogenetic stimulation suggested that there may be as many as 40 excitatory inputs and eight inhibitory inputs to LSO PNs (Gjoni et al., 2018b). At younger ages near hearing onset, ratiometric measurements obtained using electrical stimulation estimated  $\sim 5$  excitatory (Felix and Magnusson, 2016) and  $\sim 10$  inhibitory inputs (Hirtz et al. 2012, Clause et al. 2014).

The IPSCs onto inhibitory LSO PNs had slower decay kinetics (Figs. 4, 5). In absolute terms, the differences were small (0.26 ms wider for sIPSCs or 0.66 ms for eIPSCs), but in percent differences more substantial (24 and 35%). These kinetic differences may reflect variation in glycine receptor subunit expression and are the subject of future studies. In most neurons, if inhibitory synapses were located more distally, we would expect both the rise and decay to be affected which we did not observe. In medial superior olive neurons, there are ion channel-based mechanisms that help maintain the kinetics of propagated synaptic events (Mathews et al., 2010; Winters et al., 2017); however, whether such mechanisms are present in the LSO is unknown. Regardless, it is not known whether these width differences would substantially affect summation or integration of excitatory synaptic events, and it is a future direction to pursue computationally and experimentally.

Short-term synaptic plasticity can alter the impact of repetitive stimuli and thus could influence sound localization functions. We measured paired-pulse ratios at minimal stimulation intensities in an attempt to examine the interaction of successive stimulations on the same synapses and avoid the influence of recruitment/failure of subsets of fibers. Our results

suggest that LSO PN do not generally have paired-pulse interactions for IPIs as low as 5 ms. A few cells exhibited interactions in individual paired-pulse trials, but these cells did not consistently show interactions at the IPI tested. This was the case for both excitation and inhibition. A recent report, which also used minimal stimulation of inhibitory inputs to LSO PNs, showed that paired-pulse ratios in P31–49 mice were 0.88–0.92 at IPIs of 10 and 1,000 ms, suggesting little interaction (Müller et al., 2019). For younger mice at P12–22, another study found little paired-pulse interaction of minimally stimulated excitatory inputs to LSO PNs of  $\sim 0.9$ ; however, intervals longer than 20 ms were used (Felix and Magnusson, 2016). What low levels of short-term plasticity means for auditory processing is not known, but the world is rarely completely quiet, and these circuits are thought to be highly active at high rates. Being stable in the face of activity may provide benefits for information extraction. On the other hand, slices are quiet, so we do not know if in vivo short-term dynamics are different from what we observed.

We also found that the whole-cell capacitance was smaller in inhibitory LSO PNs which may contribute to their greater intrinsic membrane excitability compared with excitatory LSO PNs. These data also suggest that inhibitory LSO PNs are smaller than excitatory ones. Haragopal and Winters (2023) used z-stacks of fluorescence images to measure soma volumes and did not find differences between LSO PN transmitter types. However, there was a trend for inhibitory LSO PNs to have smaller somas. Additionally, capacitive measurements may encompass portions of the dendritic arbor and Haragopal and Winters did find that inhibitory LSO PNs had smaller/less complicated dendritic arbors. The capacitive measures we present here are also potentially more quantitative than the volumetric measurements because the fluorescence signal of very bright filled cell bodies tends to smear out in the z-axis due to the limitations of the point spread function.

Our results suggest that the greater intrinsic membrane excitability of inhibitory LSO PNs is not offset by differences in strength of synaptic drive. It is not known how having more easily excited inhibitory LSO PNs might play out in sound localization networks. Differences in activation threshold, along with transmitter type and projection laterality, may provide an additional means to segregate LSO information in higher processing centers such as the IC. It is possible that lower activation threshold would result in inhibition from LSO preceding excitation in time due to activation at smaller relative level differences. This effect could also occur from inhibitory LSO PNs having shorter spike latencies due to being driven further above their activation threshold than their excitatory counterparts. In any case, this may present a means by which inhibitory LSO PNs provide a source for “early inhibition” with shorter latency than excitation that is observed in IC neurons in vivo (Carney and Yin, 1989; Peterson et al., 2008; Voytenko and Galazyuk, 2008). The inhibitory pathway from LSO to IC is largely or entirely segregated to the ipsilateral side (Helfert et al., 1989; Saint Marie et al., 1989; Saint Marie and Baker, 1990; Glendenning et al., 1992; Henkel and Bruno-Bechtold, 1993; Ito et al., 2011; Yavuzoglu et al., 2011; Mellott et al., 2021; Haragopal et al., 2023; however, see Williams and Ryugo, 2024). Preceding either in time or relative level domain, ipsilateral inhibition may serve to sharpen the representation of auditory objects in the contralateral IC (Semple and Kitzes, 1985; Delgutte et al., 1999).

Greater understanding of the LSO→IC circuit is limited by not knowing what cell types in the IC receive inputs from LSO PN types and is an important future direction. There is however some evidence that inhibitory and excitatory LSO PNs participate in different subcircuits within the IC since ipsilateral and contralateral projections from LSO to IC target different bands or territories in cats (Shneiderman and Henkel, 1987; Loftus et al., 2004).

Although traditionally proposed to extract ILDs, LSO PNs are increasingly implicated in extraction of ITDs (for review, see Joris and Trussell, 2018; Joris and van der Heijden, 2019; Yin et al., 2019). Inhibitory LSO PNs have several intrinsic membrane properties that could provide advantages for time-coding functions. These include being more likely to present with an onset firing pattern (76%), having higher phasic spiking limit, lower maximum number of spikes, and more stable interspike intervals (Haragopal and Winters, 2023). Thus, inhibitory outputs to the ipsilateral IC from LSO may contain a preponderance of time-coding relevant information that is activated at lower sound threshold or higher sensitivity.

There is also some evidence that different types of ITD processing are segregated in the IC. ITD processing for amplitude modulations, which may be more likely to be encoded by the LSO, and fine structure ITDs which are more likely to be encoded by the medial superior olive, take place in different IC regions in gerbils (Graña et al., 2017) although it is unclear how different LSO PN cell types might be involved.

Together the work presented here suggests that inhibitory and excitatory LSO PNs have more similar synaptic inputs (with the exception of inhibitory input kinetics) than intrinsic membrane properties. Future studies will focus on specific ion channel systems involved in their intrinsic membrane differences and how differential expression may tune input/output responses for different binaural functions.

## References

- Adam TJ, Schwarz DWF, Finlayson PG (1999) Firing properties of chopper and delay neurons in the lateral superior olive of the rat. *Exp Brain Res* 124:489–502.
- Beiderbeck B, Myoga MH, Müller NIC, Callan AR, Friauf E, Grothe B, Pecka M (2018) Precisely timed inhibition facilitates action potential firing for spatial coding in the auditory brainstem. *Nat Commun* 9:1771.
- Boudreau JC, Tsuchitani C (1968) Binaural interaction in the cat superior olive S segment. *J Neurophysiol* 31:442–454.
- Cant NB (1984) The fine structure of the lateral superior olivary nucleus of the cat. *J Comp Neurol* 227:63–77.
- Carney LH, Yin TC (1989) Responses of low-frequency cells in the inferior colliculus to interaural time differences of clicks: excitatory and inhibitory components. *J Neurophysiol* 62:144–161.

- Case DT, Gillespie DC (2011) Pre- and postsynaptic properties of glutamatergic transmission in the immature inhibitory MNTB-LSO pathway. *J Neurophysiol* 106:2570–2579.
- Chen C, Song S (2024) Distinct neuron types contribute to hybrid auditory spatial coding. *J Neurosci* 44:e0159242024.
- Coomes PD, Schofield BR (2007) Projections from auditory cortex contact ascending pathways that originate in the superior olive and inferior colliculus. *Hear Res* 232:67–77.
- Couchman K, Grothe B, Felmy F (2010) Medial superior olivary neurons receive surprisingly few excitatory and inhibitory inputs with balanced strength and short-term dynamics. *J Neurosci* 30:17111–17121.
- Delgutte B, Joris PX, Litovsky RY, Yin TC (1999) Receptive fields and binaural interactions for virtual-space stimuli in the cat inferior colliculus. *J Neurophysiol* 81:2833–2851.
- Feliciano M, Saldaña E, Mugnaini E (1995) Direct projections from the rat primary auditory neocortex to nucleus sagulum, paralemniscal regions, superior olivary complex and cochlear nuclei. *Aud Neurosci* 1:287–308.
- Felix RA, Magnusson AK (2016) Development of excitatory synaptic transmission to the superior paraolivary and lateral superior olivary nuclei optimizes differential decoding strategies. *Neuroscience* 334:1–12.
- Frank MM, Sitko AA, Suthakar K, Torres Cadenas L, Hunt M, Yuk MC, Weisz CJC, Goodrich LV (2023) Experience-dependent flexibility in a molecularly diverse central-to-peripheral auditory feedback system. *Elife* 12:e83855.
- Franken TP, Joris PX, Smith PH (2018) Principal cells of the brainstem's interaural sound level detector are temporal differentiators rather than integrators. *Elife* 7:e33854.
- Franken TP, Bondy BJ, Haimes DB, Goldwyn JH, Golding NL, Smith PH, Joris PX (2021) Glycinergic axonal inhibition subserves acute spatial sensitivity to sudden increases in sound intensity. *Elife* 10:e62183.
- Fredrich M, Reisch A, Illing R-B (2009) Neuronal subtype identity in the rat auditory brainstem as defined by molecular profile and axonal projection. *Exp Brain Res* 195:241–260.
- Friauf E, Krächan EG, Müller NIC (2019) Lateral superior olive: organization, development, and plasticity. In: *The Oxford handbook of the auditory brainstem* (Kandler K, ed), pp 328–394. New York, NY: Oxford University Press.
- García-Pino E, Gesselle N, Koch U (2017) Enhanced excitatory connectivity and disturbed sound processing in the auditory brainstem of Fragile X mice. *J Neurosci* 37:7403–7419.
- Gillespie DC, Kim G, Kandler K (2005) Inhibitory synapses in the developing auditory system are glutamatergic. *Nat Neurosci* 8:332–338.
- Gjoni E, Aguet C, Sahlender DA, Knott G, Schneggenburger R (2018a) Ultrastructural basis of strong unitary inhibition in a binaural neuron. *J Physiol* 596:4969–4982.
- Gjoni E, Zenke F, Bouhours B, Schneggenburger R (2018b) Specific synaptic input strengths determine the computational properties of excitation-inhibition integration in a sound localization circuit. *J Physiol* 596:4945–4967.
- Glendenning KK, Masterton RB, Baker BN, Wenthold RJ (1991) Acoustic chiasm III: nature, distribution, and sources of afferents to the lateral superior olive in the cat. *J Comp Neurol* 310:377–400.
- Glendenning KK, Baker BN, Hutson KA, Masterton RB (1992) Acoustic chiasm V: inhibition and excitation in the ipsilateral and contralateral projections of LSO. *J Comp Neurol* 319:100–122.
- Graña GD, Hutson KA, Badea A, Pappa A, Scott W, Fitzpatrick DC (2017) The organization of frequency and binaural cues in the gerbil inferior colliculus. *J Comp Neurol* 525:2050–2074.
- Grothe B, Pecka M, McAlpine D (2010) Mechanisms of sound localization in mammals. *Physiol Rev* 90:983–1012.
- Haragopal H, Winters BD (2023) Principal neuron diversity in the murine lateral superior olive supports multiple sound localization strategies and segregation of information in higher processing centers. *Commun Biol* 6:432.
- Haragopal H, Mellott JG, Dhar M, Kanel A, Mafi A, Tokar N, Winters BD (2023) Tonotopic distribution and inferior colliculus projection pattern of inhibitory and excitatory cell types in the lateral superior olive of mice. *J Comp Neurol* 531:1381–1388.
- Helfert RH, Bonneau JM, Wenthold RJ, Altschuler RA (1989) GABA and glycine immunoreactivity in the Guinea pig superior olivary complex. *Brain Res* 501:269–286.
- Henkel CK, Brunso-Bechtold JK (1993) Laterality of superior olive projections to the inferior colliculus in adult and developing ferret. *J Comp Neurol* 331:458–468.
- Henkel CK, Brunso-Bechtold JK (1995) Development of glycinergic cells and puncta in nuclei of the superior olivary complex of the postnatal ferret. *J Comp Neurol* 354:470–480.
- Ito T, Oliver DL (2010) Origins of glutamatergic terminals in the inferior colliculus identified by retrograde transport and expression of VGLUT1 and VGLUT2 genes. *Front Neuroanat* 4:135.
- Ito T, Bishop DC, Oliver DL (2011) Expression of glutamate and inhibitory amino acid vesicular transporters in the rodent auditory brainstem. *J Comp Neurol* 519:316–340.
- Joris PX, Yin TC (1995) Envelope coding in the lateral superior olive. I. Sensitivity to interaural time differences. *J Neurophysiol* 73:1043–1062.
- Joris PX, Trussell LO (2018) The calyx of held: a hypothesis on the need for reliable timing in an intensity-difference encoder. *Neuron* 100:534–549.
- Joris PX, van der Heijden M (2019) Early binaural hearing: the comparison of temporal differences at the two ears. *Annu Rev Neurosci* 42:433–457.
- Kandler K, Clause A, Noh J (2009) Tonotopic reorganization of developing auditory brainstem circuits. *Nat Neurosci* 12:711–717.
- Lee J, Clause A, Kandler K (2023) Structural and functional development of inhibitory connections from the medial nucleus of the trapezoid body to the superior paraolivary nucleus. *J Neurosci* 43:7766–7779.
- Loftus WC, Bishop DC, Saint Marie RL, Oliver DL (2004) Organization of binaural excitatory and inhibitory inputs to the inferior colliculus from the superior olive. *J Comp Neurol* 472:330–344.
- Maraslioglu-Sperber A, Pizzi E, Fisch JO, Kattler K, Ritter T, Friauf E (2024) Molecular and functional profiling of cell diversity and identity in the lateral superior olive, an auditory brainstem center with ascending and descending projections. *Front Cell Neurosci* 18:1354520.
- Mathews PJ, Jercog PE, Rinzel J, Scott LL, Golding NL (2010) Control of submillisecond synaptic timing in binaural coincidence detectors by KV1 channels. *Nat Neurosci* 13:601–609.
- Mellott JG, Dhar M, Mafi A, Tokar N, Winters BD (2021) Tonotopic distribution and inferior colliculus projection pattern of inhibitory and excitatory cell types in the lateral superior olive of Mongolian gerbils. *J Comp Neurol* 530:506–517.
- Müller NIC, Sonntag M, Maraslioglu A, Hirtz JJ, Friauf E (2019) Topographic map refinement and synaptic strengthening of a sound localization circuit require spontaneous peripheral activity. *J Physiol* 597:5469–5493.
- Müller NIC, Paulußen I, Hofmann LN, Fisch JO, Singh A, Friauf E (2022) Development of synaptic fidelity and action potential robustness at an inhibitory sound localization circuit: effects of otoferlin-related deafness. *J Physiol* 600:2461–2497.
- Noh J, Seal RP, Garver JA, Edwards RH, Kandler K (2010) Glutamate co-release at GABA/glycinergic synapses is crucial for the refinement of an inhibitory map. *Nat Neurosci* 13:232–238.
- Ono M, Bishop DC, Oliver DL (2020) Neuronal sensitivity to the interaural time difference of the sound envelope in the mouse inferior colliculus. *Hear Res* 385:107844.
- Peterson DC, Voytenko S, Gans D, Galazyuk A, Wenstrup J (2008) Intracellular recordings from combination-sensitive neurons in the inferior colliculus. *J Neurophysiol* 100:629–645.
- Pilati N, Linley DM, Selvaskandan H, Uchitel O, Hennig MH, Kopp-Scheinpflug C, Forsythe ID (2016) Acoustic trauma slows AMPA receptor-mediated EPSCs in the auditory brainstem,

- reducing GluA4 subunit expression as a mechanism to rescue binaural function. *J Physiol* 594:3683–3703.
- Saint Marie RL, Baker RA (1990) Neurotransmitter-specific uptake and retrograde transport of [3H]glycine from the inferior colliculus by ipsilateral projections of the superior olivary complex and nuclei of the lateral lemniscus. *Brain Res* 524:244–253.
- Saint Marie RL, Ostapoff EM, Morest DK, Wenthold RJ (1989) Glycine-immunoreactive projection of the cat lateral superior olive: possible role in midbrain ear dominance. *J Comp Neurol* 279:382–396.
- Sanes DH (1990) An in vitro analysis of sound localization mechanisms in the gerbil lateral superior olive. *J Neurosci* 10:3494–3506.
- Sanes DH (1993) The development of synaptic function and integration in the central auditory system. *J Neurosci* 13:2627–2637.
- Sanes DH, Rubel EW (1988) The ontogeny of inhibition and excitation in the gerbil lateral superior olive. *J Neurosci* 8:682–700.
- Semple MN, Kitzes LM (1985) Single-unit responses in the inferior colliculus: different consequences of contralateral and ipsilateral auditory stimulation. *J Neurophysiol* 53:1467–1482.
- Shneiderman A, Henkel CK (1987) Banding of lateral superior olivary nucleus afferents in the inferior colliculus: a possible substrate for sensory integration. *J Comp Neurol* 266:519–534.
- Sterenberg JC, Pilati N, Sheridan CJ, Uchitel OD, Forsythe ID, Barnes-Davies M (2010) Lateral olivocochlear (LOC) neurons of the mouse LSO receive excitatory and inhibitory synaptic inputs with slower kinetics than LSO principal neurons. *Hear Res* 270:119–126.
- Tollin DJ (2005) Interaural phase and level difference sensitivity in Low-frequency neurons in the lateral superior olive. *J Neurosci* 25:10648–10657.
- Tsuchitani C (1977) Functional organization of lateral cell groups of cat superior olivary complex. *J Neurophysiol* 40:296–318.
- Tsuchitani C, Boudreau JC (1966) Single unit analysis of cat superior olive S segment with tonal stimuli. *J Neurophysiol* 29:684–697.
- Voytenko SV, Galazyuk AV (2008) Timing of sound-evoked potentials and spike responses in the inferior colliculus of awake bats. *Neuroscience* 155:923–936.
- Weingarten DJ, Sebastian E, Winkelhoff J, Patschull-Keiner N, Fischer AU, Wadle SL, Friauf E, Hirtz JJ (2023) An inhibitory glycinergic projection from the cochlear nucleus to the lateral superior olive. *Front Neural Circuits* 17:1307283.
- Williams IR, Ryugo DK (2024) Bilateral and symmetric glycinergic and glutamatergic projections from the LSO to the IC in the CBA/CaH mouse. *Front Neural Circuits* 18:1430598.
- Williams IR, Filimontseva A, Connelly CJ, Ryugo DK (2022) The lateral superior olive in the mouse: two systems of projecting neurons. *Front Neural Circuits* 16:1038500.
- Winters BD, Jin S-X, Ledford KR, Golding NL (2017) Amplitude normalization of dendritic EPSPs at the soma of binaural coincidence detector neurons of the medial superior olive. *J Neurosci* 37:3138–3149.
- Wu S, Kelly J (1992) Synaptic pharmacology of the superior olivary complex studied in mouse brain slice. *J Neurosci* 12:3084–3097.
- Yavuzoglu A, Schofield BR, Wenstrup JJ (2011) Circuitry underlying spectrotemporal integration in the auditory midbrain. *J Neurosci* 31:14424–14435.
- Yin TCT, Smith PH, Joris PX (2019) Neural mechanisms of binaural processing in the auditory brainstem. *Compr Physiol* 9:1503–1575.